Temple Anne Douglas[1]
Jaka Cemazar[1]
Nikita Balani[1]
Daniel C. Sweeney[1]
Eva M. Schmelz[2]*
Rafael V. Davalos[1]

[1]Bioelectromechanical Systems Laboratory, Virginia Tech-Wake Forest School of Biomedical Engineering and Sciences, Blacksburg, VA, USA
[2]Virginia Tech Department of Human Nutrition, Food and Exercise, Blacksburg, VA, USA

Received December 2, 2016
Revised March 15, 2017
Accepted March 15, 2017

Research Article

A feasibility study for enrichment of highly aggressive cancer subpopulations by their biophysical properties via dielectrophoresis enhanced with synergistic fluid flow

A common problem with cancer treatment is the development of treatment resistance and tumor recurrence that result from treatments that kill most tumor cells yet leave behind aggressive cells to repopulate. Presented here is a microfluidic device that can be used to isolate tumor subpopulations to optimize treatment selection. Dielectrophoresis (DEP) is a phenomenon where particles are polarized by an electric field and move along the electric field gradient. Different cell subpopulations have different DEP responses depending on their bioelectrical phenotype, which, we hypothesize, correlate with aggressiveness. We have designed a microfluidic device in which a region containing posts locally distorts the electric field created by an AC voltage and forces cells toward the posts through DEP. This force is balanced with a simultaneous drag force from fluid motion that pulls cells away from the posts. We have shown that by adjusting the drag force, cells with aggressive phenotypes are influenced more by the DEP force and trap on posts while others flow through the chip unaffected. Utilizing single-cell trapping via cell-sized posts coupled with a drag-DEP force balance, we show that separation of similar cell subpopulations may be achieved, a result that was previously impossible with DEP alone. Separated subpopulations maintain high viability downstream, and remain in a native state, without fluorescent labeling. These cells can then be cultured to help select a therapy that kills aggressive subpopulations equally or better than the bulk of the tumor, mitigating resistance and recurrence.

Keywords:
Biophysics / Cell separation / Heterogeneity / Microfluidics / Tumor
DOI 10.1002/elps.201600530

Additional supporting information may be found in the online version of this article at the publisher's web-site

1 Introduction

Within a tumor, there is a high degree of cellular heterogeneity due to the presence of spatially and temporally variable stressors, such as microenvironmental gradients, nutrient and oxygen concentration, and intrinsic genomic instability of the cancer cells [1–4]. As conventional cancer treatments are chosen to treat the bulk of the tumor, there exists a high probability that genetically variant subpopulations of cells will then resist a given treatment, and repopulate the tumor microenvironment following the death of nonresistant cells [5, 6]. This has been shown to correlate with a diminished efficacy of treatment over time and is responsible for a large percentage of instances of chemotherapy failure [5,7,8]. We propose a cell separating microfluidic device capable of enriching for cell types based on the intrinsic bioelectrical and biophysical properties of the cells, which we hypothesize can be eventually used to differentiate cancer cell subpopulations based on their metastatic potential. Such a device would be instrumental in developing a rapid, novel assay to

Correspondence: Professor Rafael V. Davalos, PhD, Bioelectromechanical Systems Laboratory, Virginia Tech-Wake Forest School of Biomedical Engineering and Sciences, Blacksburg, VA, USA
E-mail: davalos@vt.edu

Abbreviations: **cDEP**, contactless dielectrophoresis; **DEP**, dielectrophoresis; **FACS**, fluorescence-activated cell sorting; **IP**, intraperitoneal; **MOSE**, mouse ovarian surface epithelial; **PDMS**, polydimethylsiloxane

*Additional corresponding author: Professor Eva M. Schmelz
E-mail: eschmelz@vt.edu

© 2017 WILEY-VCH Verlag GmbH & Co. KGaA, Weinheim

provide diagnostics for personalized treatment optimization utilizing a technique called contactless dielectrophoresis (cDEP) for selective concentration for batch separation. Our device utilizes shear flow coupled with cDEP to polarize and then trap cells on a post array for batch separation. We believe that the shear flow changes the polarizability of the cell populations and thereby when optimized, enhances the separability. This device could be used to provide diagnostic information for personalized treatment optimization.

Separation of cell subpopulations from a patient tumor and subsequent selection of a chemotherapy treatment based on the composition and the degree of malignancy or metastatic potential could help direct treatment decisions and reduce instances of tumor recurrence and drug resistance, as well as prevent the development of more malignant tumors in response to chemotherapy. One current method of cell separation for this purpose is fluorescence-activated cell sorting (FACS). However, FACS relies on biomarker labeling on the cell surface, which both irreversibly modifies the cell, and limits the detection capacity to known biomarkers [9, 10]. Cells with an aggressive phenotype that lack common markers would not be detected using this method, and further downstream analysis and culture of primary cell populations would not be possible due to permanent modifications from labeling. Using our microfluidic device, cells can be separated based on their bioelectrical phenotype, which may correlate with metastatic potential of the cells. Changes in the physical structure of the outer surface membrane, the presence of membrane protrusions, nuclear to cytoplasm ratio, DNA content, and other factors may contribute to this separation. Surface labeling of cells is not necessary when using our device due to the design of insulating structures in the device. The electric field gradient is enhanced relative to the net electric field and high cellular viability is maintained [11]. Cell subpopulations can then be cultured downstream and tested against different treatments to ensure that the most aggressive cells will be effectively killed while minimizing the survival of treatment-resistant populations. In the future, clinicians could use this method to help select and optimize treatments on a case-by-case basis.

In DEP, cells become polarized in the presence of an electric field and experience a translational force parallel or anti-parallel to the electric field gradient depending on their intrinsic properties. We hypothesized that biophysical properties such as the fluidity of the membrane, presence of different transmembrane proteins, cell size, and nuclear size all influence the electrical polarizability of a given cell and dynamic response to an electric field [12–15].

Unlike traditional DEP, cDEP does not require the electrodes to be in direct contact with the cell suspension, but rather uses fluidic electrodes containing an electrolyte solution separated from the main cell-flow channel by a thin membrane. Separating the electrodes from the fluid in the device eliminates electrolysis and improves cell viability by preventing cell-to-electrode contact [16]. Analogous to insulator-based DEP (iDEP), insulating posts within the channel create gradients in the electric field that drive the DEP force [17–20]. In our case (Fig. 1), the cell-scale dimension of the posts allows for only single cells to trap and eliminates pearl chaining and clumping, phenomena that decrease trapping specificity [11, 21, 22].

We have demonstrated that by combining DEP with shear-flow in a microfluidic chip, it is possible to add an additional parameter to tune cell separation, potentially due to shear-dependent changes in cellular polarizability. To the best of our knowledge this is the first time anyone has demonstrated that shear flow coupled with DEP can add a layer of sensitivity that had been previously unachievable. This could be exploited in the future and may have potential for other applications.

Our polydimethylsiloxane (PDMS) chip consists of a main channel through which cells flow that contains an array of insulative posts, each with a diameter of 20 μm, as shown in Fig. 1. Fluidic electrodes on either side of the channel are separated from the cell channel by a 13 μm membrane and are used to apply a voltage across the chip, which causes an electric field to be established in the channel with the cells. Differences in electrical properties between the insulative posts and the buffer solution create inhomogeneities in the electric field that drive the cells to the posts, provided the applied voltage and frequency create a dielectrophoretic force that overcomes drag on the cells flowing through the device, thus trapping the cells on posts [7]. Untrapped cells continue to flow through the device and are collected at the outlet. Turning off the voltage allows the trapped cells to flow out and be collected in a separate output population.

2 Theory

In our cDEP device, drag forces on cells flowing through the microfluidic chip are balanced with the DEP force, $\vec{F}_{DEP}$, in order to accomplish cell sorting [23, 24]. The DEP force is described by:

$$\vec{F}_{DEP} = 2\pi\varepsilon_m r^3 Re\left[K(\omega)\right]\nabla\left(\vec{E}\cdot\vec{E}\right) \quad (1)$$

In this equation, ε_m is the permittivity of the medium, r is the radius of the cell, $K(\omega)$ is the Clausius–Mossotti factor that depends on the angular frequency of the applied current, ω, and $\vec{E}$ is the electric field. Different subpopulations can have differences both in the radius and in $K(\omega)$, which is defined as:

$$\mathrm{K}(\omega) = \left[\frac{\epsilon_c^* - \epsilon_m^*}{\epsilon_c^* + 2\epsilon_m^*}\right] \quad (2)$$

The complex permittivities of the cell and of the medium are ϵ_c^* and ϵ_m^*, respectively, where $\epsilon^* = \epsilon + \frac{\sigma}{i\omega}$, where ϵ is the permittivity and σ is the conductivity [23].

$\vec{F}_{DEP}$ is balanced with the drag force on the particle in the fluid. For a spherical particle in a laminar flow regime, the Stokes drag force is:

$$\vec{F}_{drag} = 6\pi\eta r\vec{v} \quad (3)$$

© 2017 WILEY-VCH Verlag GmbH & Co. KGaA, Weinheim

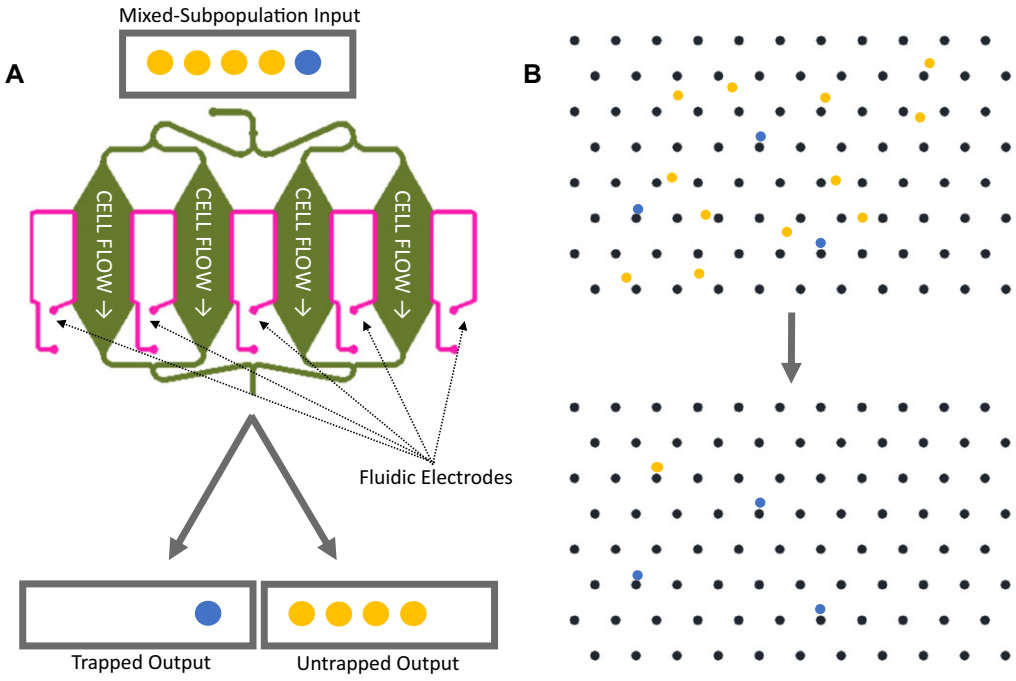

Figure 1. Schematic of microfluidic device and cells flowing through device. A mixed population of fluorescently labeled cells flow through the chip. While the voltage is on, some cells trap and others flow through. When the voltage is turned off and cells are released, trapped cells flow through resulting in two subpopulation outputs. (A) Full schematic of chip and function. (B) Post structure inside chip—cells flow through and some cells trap. When DEP buffer is sent through the chip, untrapped cells flow through, leaving only the trapped population.

In this equation, η is the fluid viscosity, r is the radius of the particle, and $\vec{v}$ is the velocity vector for the particle relative to the fluid.

3 Materials and methods

These experiments aimed to evaluate the cDEP chip design with 20 μm posts for its ability to separate out highly similar tumor cells as a model for a potential diagnostic technique. The mouse ovarian surface epithelial (MOSE) cell line was chosen as a model of a heterogeneous tumor as it is a transitional cell model with different stages of malignancy, making it ideal for subpopulation studies. From the MOSE cell line, two subcell lines of high genotypic similarity, MOSE-L_{TICv} (highly malignant, fast developing disease) and MOSE-L (slow developing disease), were used. Each cell line was labeled with red or green calcein in a concentration of 1.7 μg/mL and 5 μg/mL, respectively, and was suspended in low conductivity DEP buffer and the subpopulations were mixed together 1:4 MOSE-L_{TICv}: MOSE-L.

Optimal frequencies and voltages were found prior to conducting these experiments. Experiments were conducted from 20–40 kHz, with voltages ranging from 300–350 Vrms and flow rates from 12–36 μL/min. Using this data, it was observed that the best separation of cell lines occurred at 350 V_{rms} and 30 kHz [11]. Experiments were then conducted by changing the flowrate of the cells through the device while maintaining the found optimum frequency and voltage. Twenty-seven total trials were run at 20, 24, 28, 32, and 36 μL/min to achieve the results shown.

In each trial, 50 μL of cell suspension mixture (with less than 1 million cells/mL) was flown through the chip at different flow rates while an optimal frequency and voltage, determined by previous experiments, was applied across the chip [11]. The selected frequency of 30 kHz, close to the crossover frequency of the Clausius–Mossotti factor for each cell type, was chosen as differences between trapping efficiencies were found to be maximized at this point [11]. A voltage of 350 V_{rms} was chosen to maintain high cell viability in the output population while maximizing trapping. Cells that passed through without trapping were collected in a vial at the output. Fifty microliters of DEP buffer was sent through the chip at the same flow rate as before to wash any untrapped cells out of the device. The voltage was then turned off and trapped cells were released and washed out of the device with 50 μL of low conductivity buffer and collected in another vial, as is shown in Fig. 1A. Hemocytometry on calcein red and green labeled cells was performed to count the number of MOSE-L_{TICv} and MOSE-L cells in the trapped and untrapped populations.

3.1 Chip preparation

To make the three-layer chip, channel, and electrode layers were fabricated independently using Dow Corning Sylgard 184 PDMS with 10:1 ratio of base to cross-linker. Due to

© 2017 WILEY-VCH Verlag GmbH & Co. KGaA, Weinheim

the fine resolution in the channel layer, the mold was fabricated using deep reactive-ion etching (Bob Geil, University of North Carolina) whereas the electrode layer was fabricated using SU-8 photolithography. The thin membrane between the two layers was fabricated using a 5:1 ratio of base to cross-linker that was spun onto a silanized silicon wafer for 15 s at 500 rpm and 45 s at 4000 rpm. The membrane layer was bound to the channel and electrode layers by plasma exposure for 45 s. This set was bound to a glass slide and placed in a vacuum chamber until the time of the experiment. For additional details, refer to Cemazar et al. [11].

3.2 Cell culture

In this study, we utilized cells derived from normal MOSE cells. Via *in vitro* passaging, these cells acquired an increasingly aggressive phenotype and genotype and represent a progressive cancer cell line with different stages of the same ovarian tumor [25,26]. Late-passage (MOSE-L) represent slow growing disease (cause lethal disease in approximately 100 days after intraperitoneal (ip) injection of 1×10^6 cells) [25]. The highly aggressive MOSE-L_{TICv} was generated by ip injection of MOSE-L cells into syngeneic C57BL6 mice and harvesting of cancer cells from the ascites; these cells represent fast developing disease (1×10^4 cells cause lethal disease in 21 days) [27,28]. We found that between MOSE-L and late stage highly aggressive MOSE-L_{TICv} cells, separability was optimized at a frequency of 30 kHz. A voltage of 350 V_{rms} was applied to create a sufficiently strong electric field gradient to elicit trapping behavior.

3.3 Cell preparation

We added 1.7 μg/mL calcein red or 5 μg/mL green dye (Life Technologies) to MOSE media (High-glucose DMEM (Gibco) with 3.4 g/L added sodium bicarbonate, 1% penicillin/streptavidin, and 4% fetal bovine serum) and added this to MOSE cells (MOSE-L or MOSE-L_{TICv}, was labeled with red and the other with green calcein) in flasks and placed them in the incubator at 37° for 15 min. After dye incubation, we washed the flasks twice with phosphate buffered saline (PBS) and trypsinized cells for 3 minutes. After trypsinization, MOSE media was added to neutralize the trypsin and this suspension was pipetted into 15 mL Falcon tubes. DEP buffer (8.5% sucrose [w/v], 0.3% glucose [w/v], 0.725% RPMI [v/v]) modified with 0.1% of BSA [w/v] and 0.1% of Kolliphor P188 [w/v], and 0.1 mM EDTA was added to the Falcon tubes until a volume of 10 mL was reached. These were centrifuged at 120 g for 5 min to sediment the cells out of the suspension. The DEP buffer and media was removed and 10 mL more DEP buffer was added to the cell pellet. Two more centrifugations and DEP changes were performed. After all centrifugations, cells were suspended in 1 mL of DEP buffer without BSA/Kolliphor P118/EDTA and were pipetted through a 40 μm cell strainer to remove any cell clumps. Hemocytometry was performed and cells were suspended in more DEP buffer to 10^6 cells/mL. The two cell populations were mixed 1:4 MOSE-L_{TICv} to MOSE-L and the conductivity of the cell mixture was measured. Conductivities between 110 and 120 μS/cm were used.

3.4 Chip preparation

A chip was removed from under vacuum and ethanol was pumped through the channel layer to prime it and to prevent bubble formation. 10x PBS was put into the electrode layer channels to act as a liquid electrode. 200 μL pipette tips were placed in the electrode channel outlets and filled with 10x PBS as well. A syringe full of DEP buffer was attached to one of the inlet holes via 30-gauge tubing and DEP buffer was run through the chip to remove the ethanol. A syringe full of the cell mixture was attached to the other inlet with 30-gauge tubing. Each of the syringes was placed on a syringe pump to control speed of pumping through the device. Output liquid was sent through 30-gauge tubing and collected in a 0.75 mL microcentrifuge tube.

3.5 cDEP setup

A waveform generator (Agilent 33500B Series) was used to send a sinusoidal wave to a high voltage amplifier (Trek Model 2205) where it was amplified to the desired voltage to be sent to the chip. An oscilloscope (Tektronix DPO 2012 Digital Phosphor Oscilloscope) was used to monitor the voltage. Two syringe pumps (Harvard Apparatus Pump 11 Elite and Harvard Apparatus PhD Ultra) were used to pump DEP buffer and medium into the chips. The Pump 11 Elite pump has a handheld unit that was positioned on a ring stand at an angle above the chip to ensure cells enter the chip uniformly.

3.6 cDEP experiments

Before the experiment, 50 μL of the cell mixture was pumped through the device at the target flow rate with no applied voltage and cells were collected at the outlet to be the control population for the experiment. During the cDEP experiment, cells were pumped through the chip at the assigned flow rate, voltage, and frequency up to the target volume of 50 μL. Some cells flowed through the device and into a microcentrifuge tube while others remained in the chip trapped on posts. While leaving the voltage on, 50 μL of the DEP buffer was flown through the chip to wash out any untrapped cells. Then, the microcentrifuge tube at the outlet was changed, the voltage was turned off and 50 μL of DEP buffer was flown through to wash out the trapped cells. After a run was completed, the cells in the syringe were pumped out and reloaded to prevent settling between runs.

© 2017 WILEY-VCH Verlag GmbH & Co. KGaA, Weinheim

3.7 Imaging

Per run, two microcentrifuge tubes containing the trapped and untrapped populations were obtained. Ten microliters of each output population was pipetted onto a hemocytometer and imaged with fluorescent microscopy. The number of red calcein and number of green calcein cells in each output population was counted and compared to the original control population.

3.8 Analysis

Cells were counted both manually using the ImageJ multipoint tool, and automatically using Analyze Particles.

3.9 Normalization

In order to normalize by the initial population to account for experimental error in mixing cells together, the fraction of MOSE-L_{TICv} in the trapped population ($\boldsymbol{X}_{trapped}$) and untrapped populations ($\boldsymbol{X}_{untrapped}$) was divided by the fraction of MOSE- L_{TICv} in the initial population ($\boldsymbol{X}_{initial}$):

$$\tilde{\boldsymbol{X}}_{trapped} = \frac{\boldsymbol{X}_{trapped}}{\boldsymbol{X}_{initial}}$$

$$\tilde{\boldsymbol{X}}_{untrapped} = \frac{\boldsymbol{X}_{untrapped}}{\boldsymbol{X}_{initial}}$$

In these quantities, a value of $\tilde{\boldsymbol{X}}_{trapped} = 1$ or $\tilde{\boldsymbol{X}}_{untrapped} = 1$ indicates no change in proportion of MOSE- L_{TICv} cells between the sorted and unsorted populations. A value of 2 would indicate that the sorted population had doubled its amount of MOSE-L_{TICv} cells when compared with the initial population. Propagation of error equations were utilized to find the normalized standard deviations ($\tilde{\boldsymbol{\sigma}}_X$):

$$\tilde{\boldsymbol{\sigma}}_{X_{trapped}} = \tilde{\boldsymbol{X}}_{trapped}\sqrt{\left(\frac{\boldsymbol{\sigma}_{X_{trapped}}}{\boldsymbol{X}_{trapped}}\right)^2 + \left(\frac{\boldsymbol{\sigma}_{Xinitial}}{\boldsymbol{X}_{initial}}\right)^2}$$

$$\tilde{\boldsymbol{\sigma}}_{X_{untrapped}} = \tilde{\boldsymbol{X}}_{untrapped}\sqrt{\left(\frac{\boldsymbol{\sigma}_{X_{untrapped}}}{\boldsymbol{X}_{untrapped}}\right)^2 + \left(\frac{\boldsymbol{\sigma}_{Xinitial}}{\boldsymbol{X}_{initial}}\right)^2}$$

3.10 Measurement of nucleus to cytoplasm ratio

Cell and nucleus size measurements were obtained through fluorescence microscopy using MOSE cells stained with Calcein AM to resolve the cytoplasm and NucBlue to resolve the nucleus. Staining was performed using a solution of 1 μL of Calcein AM stock (Life Technologies, Eugene, Oregon, USA) and two drops of NucBlue (Life Technologies) added to the T-25 flasks for every 1 mL of growth medium. Cells were incubated at 37°C and 5% CO_2 for 45 min to allow the vital stains to enter the cells. Following staining, cells were trypsinized, spun at 125 g for 6 min, and resuspended in low-conductivity DEP buffer as described above. Twenty microliters of the cell suspension was then transferred to a glass slide and a coverslip was wet-mounted on top of the cell sample. Brightfield images were obtained through a 63x/0.70 dry objective while fluorescence images were obtained by exciting the labeled cells using 470 ± 20 nm and reading at 525 ± 25 nm for the calcein stain and excited at 350 ± 25 nm and read at 460 ± 25 nm for the NucBlue stain. Imaging was performed using a Leica DMI6000B inverted fluorescence microscope (Leica Microsystems, Bannockburn, IL, USA) equipped with a Hamamatsu C9100-02 EMCCD camera (Hamamatsu Photonics, Shizuoka Pref., Japan). The nucleus and cell radius were measured using a purpose-written ImageJ plugin that identifies high-fluorescence intensity regions of the Calcein AM stained cells in the green channel to identify the cell boundary, then searches the blue channel for a NucBlue-stained region with high-fluorescence intensity contained within the identified cell boundary. This interior boundary was identified as the nucleus. The cell and nuclear radii were determined as the square root of the product of the major and minor radii for each the nucleus and the cell and the nucleus-to-cytoplasm ratio was taken to be the cubed ratio of nuclear radius to the cell radius.

4 Results and discussion

The percentage MOSE-L_{TICv} (highly malignant) cells as a proportion of total cell count for each of the populations is shown in Fig. 2. Interestingly, we found that as the flow rate was optimized, the trapping ratio between the two subpopulations was increased. This increased sensitivity of the device could allow for separation of highly similar cells by increasing the drag force on the cells to a comparable magnitude to that of the DEP force. At higher flow rates, the magnitude of the drag force in proportion to the DEP force (Eq. (1)) increases, and could contribute to the enhanced force balancing that is seen in the chip. The cellular polarizability could have a shear-dependent component as well. The MOSE-L_{TICv} cells trapped at a higher rate than the MOSE-L cells. At 32 μL/min, the trapped population contained 41% MOSE-L_{TICv} compared to 23% MOSE-L_{TICv} in the untrapped population. The increase in trapping efficiency leveled between 32 and 36 μL/min, indicating an optimal flow rate to maximize separability. This indicates that our device is able to detect fine differences between cells based on bioelectrical phenotype. Several factors can contribute to this difference in trapping efficiency at the given frequency, including cell polarizability, radius, transmembrane proteins, lipid bilayer structure and rigidity and cytoplasm content [29].

Changing the applied frequency is one way to enhance separation between two populations, but frequency-dependent enhancement is not possible beyond a finite optimal frequency range. However, changing the flow rate of the cells and media through the device modifies the drag force on trapped and untrapped cells and can tip the force balance to prevent cells experiencing a weak DEP force from trapping. For cells of radius r at a given point in the microfluidic chip

© 2017 WILEY-VCH Verlag GmbH & Co. KGaA, Weinheim

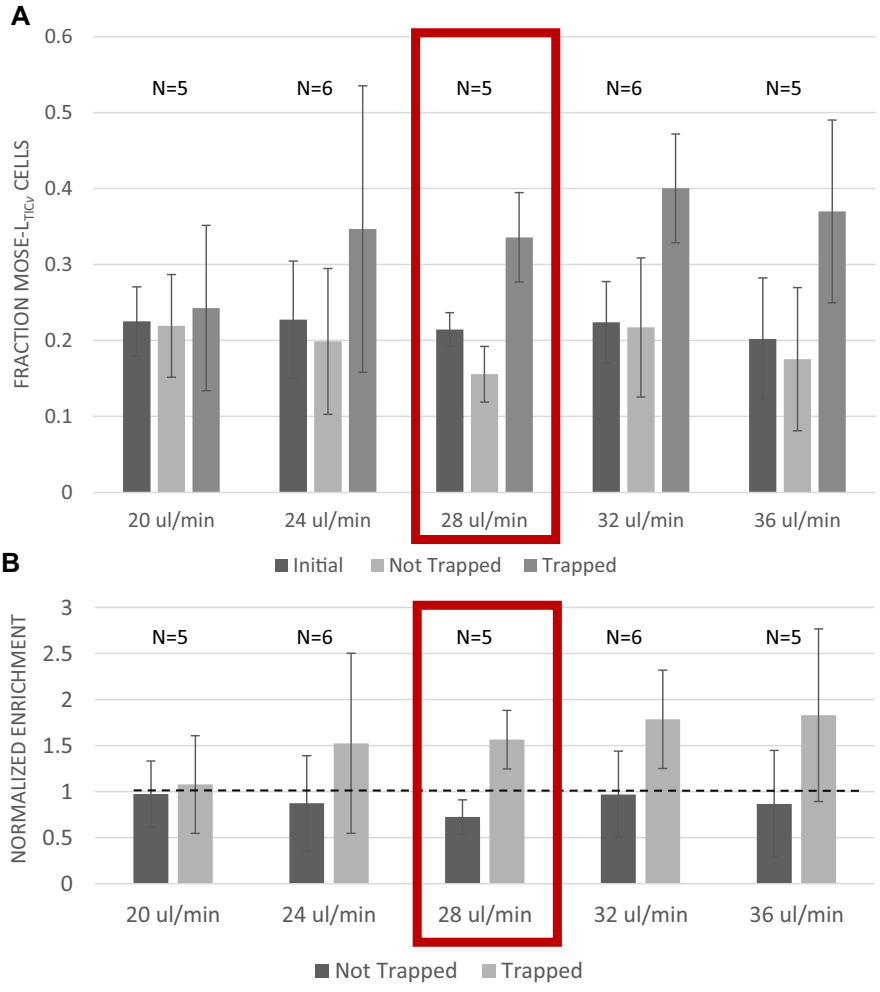

Figure 2. (A) Percentage of highly malignant MOSE-L$_{TICv}$ cells in the output populations compared to the initial and untrapped populations at 350 Vrms, 30 kHz applied voltage and different flow rates. *N* shows the number of trials at each flow rate. (B) Separation data normalized by the initial population, to show percentage enhancement for each population.

with a defined electric field gradient (for example, in front of a post), the force on that cell is proportional to $Re\{K(\omega)\}$. Comparing a highly polarizable cell with a less polarizable cell of equal radius at a given location and given $\nabla(\vec{E}\cdot\vec{E})$, the force on the highly polarizable cell is greater than the force on the less polarizable cell. If the velocity of the medium relative to the cell is such that the drag force is increased, it is possible to find an optimal flow rate at which the more polarizable cells become trapped while less polarizable cells cannot maintain their location on the posts and fall off.

We used fluorescence microscopy to observe static cell suspensions in DEP buffer and found that the MOSE-L$_{TICv}$ cells and MOSE-L cells statistically differ in both their nucleus-to-cytoplasm ratio (NCR) as well as in their radius, as is shown in Fig. 3. The cell radius for the MOSE-L$_{TICv}$ cells is larger on average than that for the MOSE-L cells. In addition, the MOSE-L cells appear to have subpopulations within the in vitro culture with smaller radii. The MOSE-L$_{TICv}$ cells appear to have a small subpopulation that has an average radius larger than the rest of the population. These subpopulations within the transitional cell lines could be indicative of further divergent evolutionary pathways due to the in vivo allografted culture environment. Plotting the NCR ratio against cell radius parameter space in Fig. 3, we see that the two cell types occupy very different regions that could also indicate varied differences in bioelectrical phenotype, related to the observed differences in trapping. Additional NCR data on earlier stages of this cell line is found in Supporting Information Fig. 1. However, differences in nucleus to cytoplasm ratio do not significantly contribute to differences in the Clausius–Mossotti factor, indicating that separation must also be based on differences in bioelectrical phenotype as well as geometry.

Some degree of heterogeneity should be expected in any cell population. For highly similar cell populations, 100% separability likely would not occur, as the phenotype distribution of one subpopulation and of the other subpopulation will overlap to some degree. Some cells within the less malignant MOSE-L population will have some probability of becoming more aggressive and similar to MOSE-L$_{TICv}$ due to *in vitro* adaptation, and some cells within the highly malignant MOSE-L$_{TICv}$ population might have characteristics that more closely match to the MOSE-L population. However, if the chip is able to enrich subpopulations in different

© 2017 WILEY-VCH Verlag GmbH & Co. KGaA, Weinheim

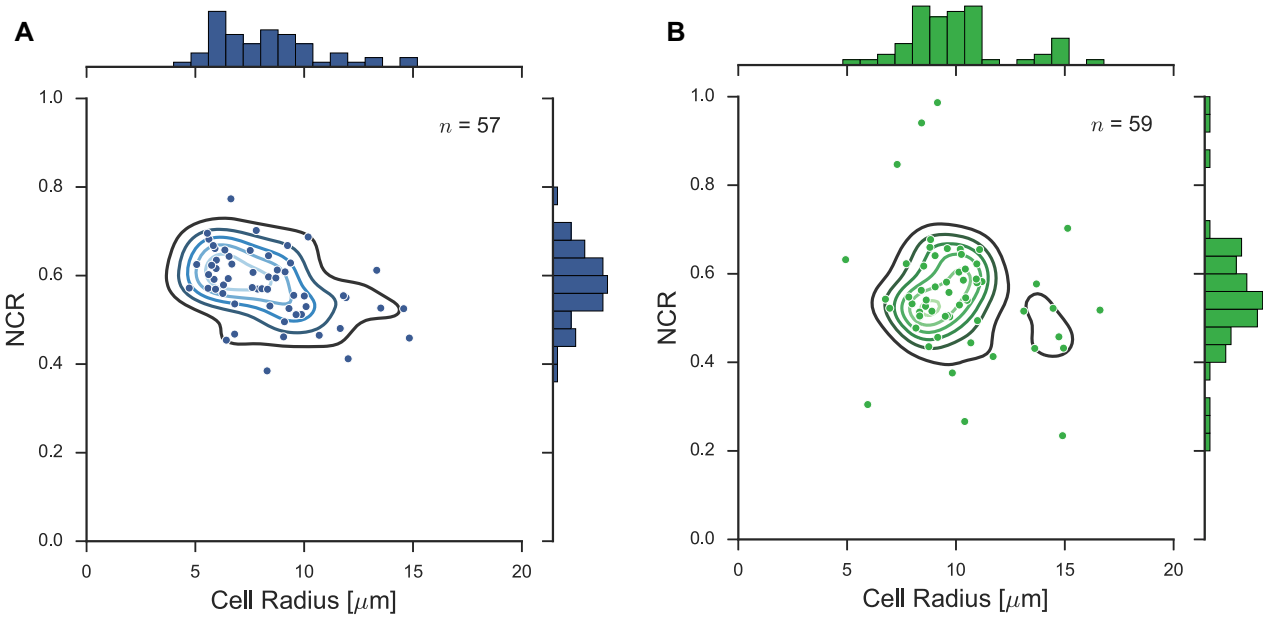

Figure 3. (A) Cell radius and nucleus-to-cytoplasm ratio (NCR) for MOSE-L cells. (B) Cell radius and NCR for MOSE-L_{TICv} cells. MOSE-L_{TICv} compared to MOSE-L cells have larger radii on average and a more uniform cell radius for the population compared to MOSE-L cells, which appear to have divergent characteristics around a smaller radius. MOSE-L_{TICv} cells also have a lower nucleus to cytoplasm ratio than MOSE-L cells on average.

proportions from the initial cell population given that the average malignancy for the MOSE-L and MOSE-L_{TICv} cell cultures differ, then the chip is able to sufficiently distinguish between the cell populations by phenotype even though the possibility of 100% separability may not exist. These subpopulations, once off-chip, can be studied and different treatments can be tested against them, as a differential rate of cell death due to a certain treatment in each of the off-chip populations will correlate with the higher proportion of cells in that off-chip subpopulation.

In previous studies, we have shown that because the DEP force is dependent on the gradient of the electric field squared rather than its magnitude, using 20-μm posts in the device improves separation specificity by reducing cell clumping and pearl chaining, a process involving a strand of cells forming in response to the DEP force. Cell-size posts also maintain high viability in the output population by maximizing the ratio $\nabla|\vec{E}|^2/|\vec{E}|$ while still being large enough to trap cells [11]. By limiting to single or two cell trapping, as shown in Fig. 1B and combining this with flow rate dependent sorting, highly similar cells are able to be separated with a high degree of specificity while maintaining very high viability in the output population. This flow-rate DEP separation adds a new technique to the toolbox of DEP researchers.

5 Concluding remarks

Using our microfluidic device, we were able to separate highly similar cell lines based on their bioelectrical differences. These cell lines originated from the same cell line source, and therefore provide an *in vitro* model that can replicate behavior expected during evolution of tumor heterogeneity *in vivo*. We showed that by optimizing flow rate in the device, force balancing on cells is improved and can lead to higher separability of cells with similar bioelectrical phenotype, a result previously not shown in dielectrophoresis.

The use of shear flow add to the armamentarium of DEP researchers for enhanced cell separation for their particular application, by providing another parameter that can be controlled to optimize separation and characterization.

This work was supported by NIH 5R21 CA173092-01, Isolation and enrichment of tumor stem cells using contactless dielectrophoresis and CIT MF13-037-LS, Use of Electric Fields for the Isolation of Tumor Initiating Cells and Other Rare Cells. We would also like to acknowledge Virginia Biosciences Health Research Corporation (VBHRC) and NSF IGERT DGE-0966125 MultiSTEPS.

The authors have patents in the field of dielectrophoresis.

6 References

[1] Zhao, Z., Zhao, B., Bai, Y., Iamarino, A., Gaffney, S. G., Schlessinger, J., Lifton, R. P., Rimm, D. L., Townsend, J. P., Proc. Natl. Acad. Sci. USA 2016, *113*, 2140–2145.

[2] Rutledge, S. D., Douglas, T. A., Nicholson, J. M., Vila-Casadesús, M., Kantzler, C. L., Wangsa, D., Barroso-Vilares, M., Kale, S. D., Logarinho, E., Cimini, D., *Sci. Rep.* 2016, *6*, 22828.

[3] Drasdo, D., Höhme, S., *Phys. Biol.* 2005, *2*, 133–147.

© 2017 WILEY-VCH Verlag GmbH & Co. KGaA, Weinheim

[4] Swanton, C., *Cancer Res.* 2012, *72*, 4875–4882.

[5] Wodarz, D., *Biol. Theory* 2006, *1*, 119–122.

[6] Gerlinger, M., Rowan, A. J., Horswell, S., Larkin, J., Endesfelder, D., Gronroos, E., Martinez, P., Matthews, N., Stewart, A., Tarpey, P., Varela, I., Phillimore, B., Begum, S., McDonald, N. Q., Butler, A., Jones, D., Raine, K., Latimer, C., Santos, C. R., Nohadani, M., Eklund, A. C., Spencer-Dene, B., Clark, G., Pickering, L., Stamp, G., Gore, M., Szallasi, Z., Downward, J., Futreal, P. A., Swanton, C., *N. Engl. J. Med.* 2012, *366*, 883–892.

[7] Galluzzi, L., Senovilla, L., Vitale, I., Michels, J., Martins, I., Kepp, O., Castedo, M., Kroemer, G., *Oncogene* 2012, *31*, 1869–1883.

[8] Gatenby, R. A., Silva, A. S., Gillies, R. J., Frieden, B. R., *Cancer Res.* 2009, *69*, 4894–4903.

[9] Bonner, W. A., Hulett, H. R., Sweet, R. G., Herzenberg, L. A., *Rev. Sci. Instrum.* 1972, *43*, 404–409.

[10] Gagnon, Z. R., *Electrophoresis* 2011, *32*, 2466–2487.

[11] Čemažar, J., Douglas, T. A., Schmelz, E. M., Davalos, R. V., *Biomicrofluidics* 2016, *10*, 014109.

[12] Pethig, R., Kell, D. B., *Phys. Med. Biol.* 1987, *32*, 933–970.

[13] Čemažar, J., Kotnik, T., *Electrophoresis* 2012, *33*, 2867–2874.

[14] Chan, K. L., Gascoyne, P. R. C., Becker, F. F., Pethig, R., *Biochim. Biophys. Acta.* 1997, *1349*, 182–196.

[15] Pethig, R., *Biomicrofluidics* 2010, *4*, 022811.

[16] Saucedo-Espinosa, M. A., LaLonde, A., Gencoglu, A., Romero-Creel, M. F., Dolas, J. R., Lapizco-Encinas, B. H., *Electrophoresis* 2016, *37*, 282–290.

[17] Lapizco-Encinas, B. H., Simmons, B. A., Cummings, E. B., Fintschenko, Y., *Electrophoresis* 2004, *25*, 1695–1704.

[18] Cummings, E. B., Singh, A. K., *Anal. Chem.* 2003, *75*, 4724–4731.

[19] Ajdari, A., Prost, J., Proc. Natl. Acad. Sci. USA 1991, *88*, 4468–4471.

[20] Cabodi, M., Chen, Y., Turner, S. W. P., Craighead, H. G., Austin, R. H., *Electrophoresis* 2002, *23*, 3496–3503.

[21] Salmanzadeh, A., Romero, L., Shafiee, H., Gallo-Villanueva, R. C., Stremler, M. A., Cramer, S. D., Davalos, R. V., *Lab Chip* 2012, *12*, 182–189.

[22] Sano, M. B., Salmanzadeh, A., Davalos, R. V., *Electrophoresis* 2012, *33*, 1938–1946.

[23] Kirby, B. J., *Micro- and Nanoscale Fluid Mechanics: Transport in Microfluidic Devices*, Cambridge University Press, Cambridge, UK 2013.

[24] Pohl, H. A., *Dielectrophoresis: The Behavior of Neutral Matter in Nonuniform Electric Fields*, Cambridge University Press, Cambridge, UK 1978.

[25] Salmanzadeh, A., Elvington, E. S., Roberts, P. C., Schmelz, E. M., Davalos, R. V., *Integrative Biol.* 2013, *5*, 843–852.

[26] Creekmore, A. L., Silkworth, W. T., Cimini, D., Jensen, R. V., Roberts, P. C., Schmelz, E. M., *PLoS One* 2011, *6*, e17676.

[27] Cohen, C. A., Shea, A. A., Heffron, C. L., Schmelz, E. M., Roberts, P. C., *PLoS One* 2013, *8*, e66477.

[28] Cohen, C. A., Shea, A. A., Heffron, C. L., Schmelz, E. M., Roberts, P. C., *Cancer Prev. Res.* 2013, *6*, 11.

[29] Pethig, R., *Adv. Drug Deliv. Rev.* 2013, *65*, 1589–1599.

© 2017 WILEY-VCH Verlag GmbH & Co. KGaA, Weinheim